Journal of Ceramic Processing Research. Vol. 22, No. 6, pp. 675~678 (2021)
(Received 28 June 2021, Received in revised form 8 September 2021, Accepted 11 September 2021)
https://doi.org/10.36410/jcpr.2021.22.6.675

J O U R N A L O F
Ceramic Processing Research

Effect of LiF addition on the sinterability, crystal structure and microwave dielectric properties of $Li_3Mg_4NbO_8$ ceramics

Wei Jin, Jingjing Tan, Jiaxin Yan, Yao Tao, Ningning Yao, Xiaomeng Ruan and Cuijin Pei*
School of Science, Xi'an University of Posts and Telecommunications, Xi'an 710121, China

The normative solid-state reaction process was adopted to prepare $Li_3Mg_4NbO_8$ ceramics with LiF addition. We investigated the impacts of LiF additive on the crystal structure, sinterabillity as well as dielectric performance at microwave region of the $Li_3Mg_4NbO_8$-basic ceramics. XRD analysis confirmed that the addition of LiF to $Li_3Mg_4NbO_8$ lead to the formation of new phase $Li_4Mg_4NbO_8F$ with cubic rock salt structure. The densified temperature of $Li_3Mg_4NbO_8$-basic ceramics could be effectively reduced from 1150 °C to 900 °C with LiF addition. Both the permitivity (ε_r) and quality factor (Qf) of present ceramics were is closely correlated with the bulk density and cell volume. The 900 °C-sintered $Li_3Mg_4NbO_8$-basic ceramics owned excellent chemical compatibility with silver and optimized microwave dielectric performance (ε_r ~13. 4, Qf ~ 32,400 GHz at 9.4 GHz, and temperature coefficient of resonant frequency (τ_f) ~ -43.0 ppm/°C).

Keywords: Ceramics, $Li_3Mg_4NbO_8$, crystal structure, microwave dielectric properties

Introduction

With the arrival of 5G communication systems, more attention has been attracted to microwave dielectric ceramics, which is extensively applied in modern communication field. Meanwhile, a series of sintering synthetic approaches, for example the cold sintering process and low-temperature co-fired ceramic (LTCC) technology, furnish technical support to produce the multi-functional, and miniaturized passive microwave devices [1-4]. Thus, the dielectric ceramics applied in 5G and LTCC technologies must fulfill the following essential basic characteristics: low firing temperature (≤960 °C), good dielectric performance as well as low-cost and environmental friendly [5]. At present, a great number of studies were taken to lower the sintering temperature of existing ceramics or exploit novel ceramic systems with good microwave dielectric performance and low firing temperature [6-10].

Recently, rock salt structural Li_2O-MgO-Nb_2O_5 system ceramics have drawn great attentions due to their intriguing dielectric and luminescence performance [11-14]. More recently, our group reported the microwave dielectric performance of a new phase ($Li_3Mg_4NbO_8$) in Li_2O-MgO-Nb_2O_5 system [15]. However, the major challenge of $Li_3Mg_4NbO_8$ ceramics is its high sintering temperature, which impeded its practical use to some extent, especially in LTCC technology. Usually, the reduction of sintering temperature of ceramics could be achieved by two methods: viz. (i) Using highly active nanopowders synthesized by wet chemical route. (ii) Adding sintering aid with low melting point [16]. Among them sintering aid addition is the most economical and effective approach [17]. It is reported that LiF is an effective firing additive for reducing the sintering temperature of many ceramics due to its low melting point of 848 °C [18-20]. What's more, LiF with other oxides materials (Li_2TiO_3, Li_3NbO_4, $Li_3Mg_2NbO_6$) with the same rock salt structure can easily form a new oxy-fluoride compound, which can facilitate a remarkable decrease in the sintering temperature of the oxides materials [21-23]. In present paper, the LiF was selected to make the $Li_3Mg_4NbO_8$ ceramic be used as a LTCC material. Then we examined systematically the impacts of LiF on the crystal phase constitution, firing behavior, microstructures, microwave dielectric characterization, and chemical compatibility with silver of $Li_3Mg_4NbO_8$ ceramics.

*Corresponding author:
Tel : +86 29 88166089
Fax: +86 29 88166333
E-mail: pcj0125@163.com

Experimental

The $Li_3Mg_4NbO_8$-LiF ceramics were elaborated through the normative process route of solid-state reaction. The high purity powders (LiF, Li_2CO_3, MgO, Nb_2O_5) were weighed according to stoichiometric $Li_3Mg_4NbO_8$, and pre-milled for 8 h using alcohol and zirconia balls as grinding media. The dried slurries were pre-sintered at 1000 °C during 4 h in order to form the $Li_3Mg_4NbO_8$ phase. Subsequently, $Li_3Mg_4NbO_8$-LiF mixture powders were re-milled for 8 h. Green discs (Φ10×5 mm) were prepared with a pressure of 100 MPa and using the mixture of $Li_3Mg_4NbO_8$-LiF

mechanically milled powders and Polyvinyl alcohol (6 wt%). These discs were fired at 850-950 °C for 5 h in air.

Phase assemblages for $Li_3Mg_4NbO_8$-LiF ceramics were analyzed by Powder X-ray diffraction (XRD, Smartlab, Japan). Use the Hitachi SU3800 scanning electron microscope to observe the microstructures of $Li_3Mg_4NbO_8$-LiF ceramics. The bulk densities of present ceramics were measured through the method of Archimedes. Use Rohde & Schwarz ZNB20 vector network analyzer and resonant cavity method to measure the dielectric performance (ε_r, Qf) of $Li_3Mg_4NbO_8$-LiF sintered bodies at around 9-10 GHz. The τ_f value was calculated using the following formula (1).

$$\tau_f = \frac{(f_{80} - f_{20}) \times 10^6}{f_{20} \times (80 - 20)} \quad (1)$$

where f_{80} and f_{20} mean the measured frequency under 80 and 20 °C, respectively.

Results and Discussion

Fig. 1 displays the XRD profiles for $Li_3Mg_4NbO_8$-LiF samples fired at 850-950 °C. The major diffraction peaks can be ascribed to the standard diffraction lines of cubic-type MgO (PDF#87-0651) phase rock salt structure, while the other diffraction peaks can well indexed to orthorhombic-type $Li_3Mg_4NbO_8$ phase rock salt structure. And no obvious LiF or impurity phase was formed, except for the cubic and orthorhombic ($Li_3Mg_4NbO_8$) phases, indicating that LiF diffused into the orthorhombic structure phase $Li_3Mg_4NbO_8$ and formed the new phase ($Li_4Mg_4NbO_8F$) with cubic structure. The similar phenomenon was also found in previous researches [23]. The cubic type structure is the consequence of a disordered sub-cell of the orthorhombic superstructure [24]. In addition, the enlarged main peak (200) moved to lower angle with rising sintering temperature as illustrated in Fig. 1(b), indicating an expansion of cell volume based on the Bragg equation ($2d \sin\theta = n\lambda$).

Typical surface SEM images for $Li_3Mg_4NbO_8$-LiF ceramics fired at 875-950 °C are displayed in Fig. 2. Some open pores were observed for the samples fired below 900 °C, as seen in Figs. 2(a) and (b). With the enhancement of firing temperature, the open pores gradually decrease and a relative compact and homogeneous microstructure were obtained for the specimen fired at 900 °C (Fig. 2(b)). However, when the firing temperature exceeded 925 °C, partial grains begin to melt due to over-firing as seen in Figs. 2(c) and (d), which inevitably affects the bulk density and dielectric performance of investigated ceramics [25].

Fig. 3 presents the dependence of bulk density (ρ), ε_r, Qf and τ_f on sintering temperature for $Li_3Mg_4NbO_8$-LiF

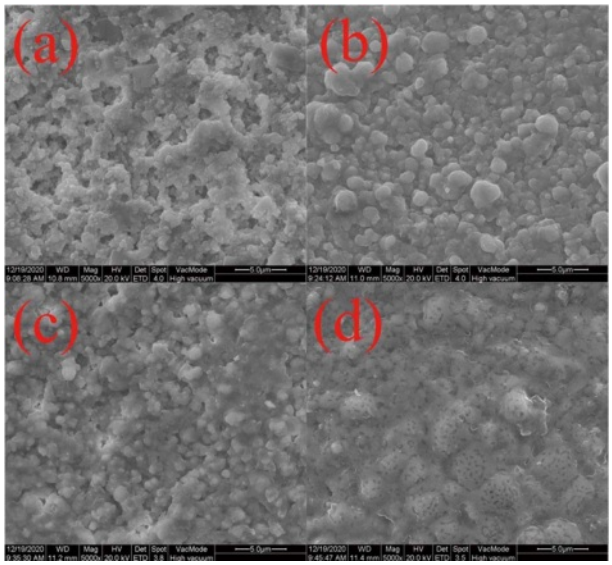

Fig. 2. SEM images of $Li_3Mg_4NbO_8$-LiF ceramics sintered at different temperatures: (a) 875 °C, (b) 900 °C, (c) 925 °C, (d) 950 °C.

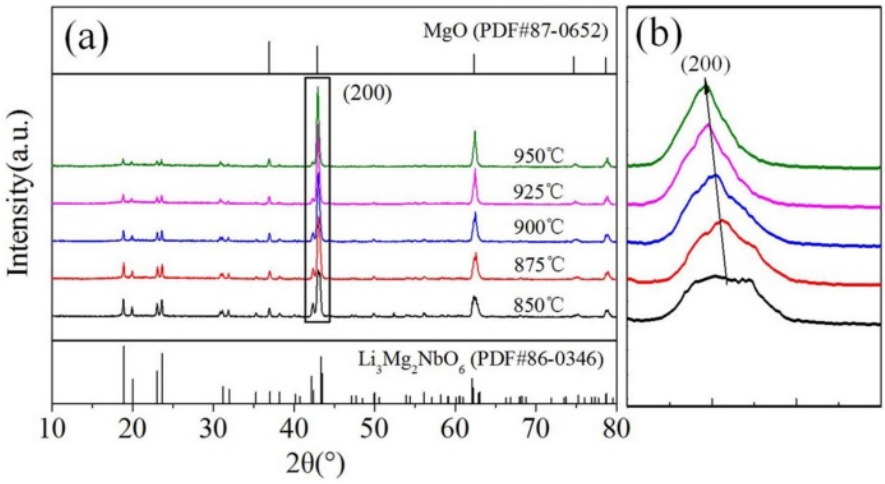

Fig. 1. (a) XRD patterns of $Li_3Mg_4NbO_8$-LiF ceramics sintered at different temperatures, (b) enlarged view of the (200) peak.

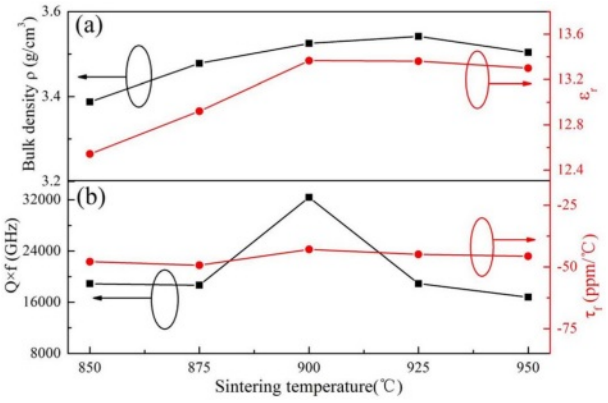

Fig. 3. The bulk density (ρ), ε_r, Qf and τ_f values of $Li_3Mg_4NbO_8$-LiF ceramics sintered at 850-950 °C.

specimens. With enhancing firing temperature from 850 to 925 °C, the ρ enhanced gradually from 3.387 to 3.542 g/cm^3, but then declined to 3.50 g/cm^3 at 950 °C. The elevating sintering temperature can simultaneously cause contradictory effects that are attributed to an enhanced ρ due to the confined porosity and related to a decreased ρ due to over-sintering associated with the partial grains melting mentioned before. From the view point of ρ, the firing temperature of the $Li_3Mg_4NbO_8$-basic ceramics was markedly reduce from 1150 °C to 925 °C with the additive of LiF [15]. LiF diffused into the $Li_3Mg_4NbO_8$ lattice, which reduced the chemical potential of $Li_3Mg_4NbO_8$. The combination of the formation of low melting point liquid phase during sintering process and the alleviation of chemical potential was responsible for the low temperature sintering of the $Li_3Mg_4NbO_8$-LiF system [26]. As illustrated in Fig. 3(b), both the ε_r and Qf values for $Li_3Mg_4NbO_8$-LiF ceramics rose initially, achieved a peak at 900 °C and thereafter decreased with rising firing temperature. The variations were somewhat inconsistent with of bulk density, implying that except ρ, other factors impacting the ε_r and Qf values should be considered. Generally, the ε_r is associated with the presence of secondary phase, bulk density, mean ionic polarization (α_{theo}/V_m) [27]. From Fig. 1, there was no secondary phase in all samples, but the cell volume (V_m) increased as rising firing temperature and thus resulted in the decline of α_{theo}/V_m. Therefore, the variation of ε_r could be explained by the competing results of bulk density and α_{theo}/V_m. Regarding Qf: it is tightly connected with the packing fraction (P.F.) and density. High P.F. corresponds to the weak lattice vibration and thus high Qf value [28]. In this work, with increasing temperature the P.F. decreased due to the enhanced cell volume (Fig. 1(b)) based on the formula (2).

$$\text{Packing fr action} = \frac{\text{volume of packed ions}}{\text{volume of unit cell}} \times Z \quad (2)$$

Thus, the variation of Qf for present ceramics could be ascribed to the combined effects of bulk density and P.F.

To evaluate its potential applications in LTCC technology, the chemical compatibility between Ag electrode and $Li_3Mg_4NbO_8$-LiF ceramics was investigated. Fig. 4 exhibits the results of XRD profile as well as SEM-EDS of $Li_3Mg_4NbO_8$-LiF with 20 wt% Ag addition sintered at 900 °C. The XRD pattern in Fig. 4 shown that only diffraction peaks for $Li_4Mg_4NbO_8F$/$Li_3Mg_4NbO_8$ and Ag (JCPDS# 89-3722) phases were detected, indicating no chemical reaction occurred between $Li_3Mg_4NbO_8$ and Ag. In addition, from the insert of Fig. 4, the clear interface and relatively tightly bonded between $Li_3Mg_4NbO_8$-LiF and Ag phases were observed, indicating no diffusion occurred between them during the firing process. These results demonstrated that the $Li_3Mg_4NbO_8$-LiF ceramics exhibited excellent Ag-cofiring chemical compatibility and thus is a potential candidate for LTCC applications.

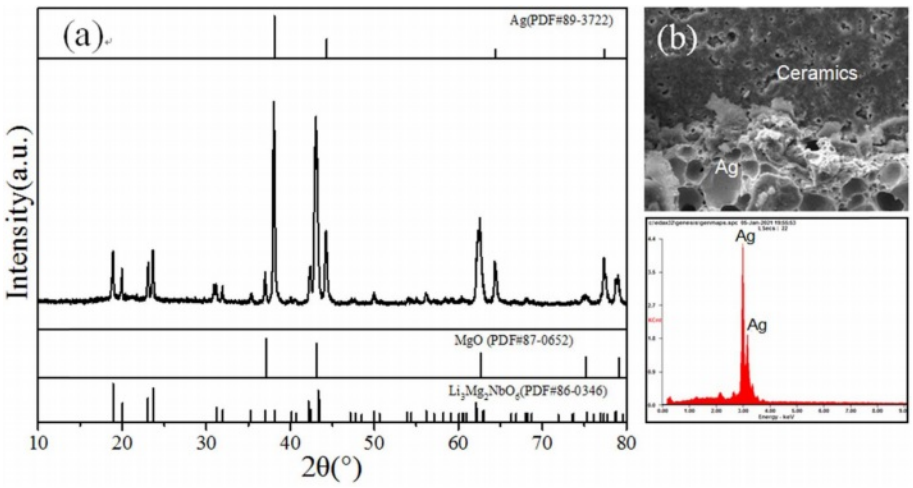

Fig. 4. (a) XRD, (b) fracture SEM-EDS analysis of $Li_3Mg_4NbO_8$-LiF ceramics co-fired with 20 wt% Ag powders at 900 °C.

Conclusions

The influences of LiF doping on the sintering behavior, crystal phase constitution, and dielectric performance at microwave frequency for $Li_3Mg_4NbO_8$ had been researched. The doping of LiF significantly lowed its densification temperature of $Li_3Mg_4NbO_8$-basic ceramics. The mixed cubic ($Li_4Mg_4NbO_8F$) and orthorhombic ($Li_3Mg_4NbO_8$) phases with rock salt structure were revealed via XRD analysis. Both the Qf and ε_r values were strongly depended on the cell volume and bulk density of ceramics. The $Li_4Mg_4NbO_8F$-$Li_3Mg_4NbO_8$ ceramics fired under 900 °C owned optimized dielectric performance at about 9.4 GHz (Qf = 32,400 GHz, ε_r = 13. 4, τ_f = -43.0 ppm/°C) along with good Ag-cofiring chemical compatibility, suggesting it a latent material for LTCC applications.

Acknowledgements

The authors acknowledge supports from National Natural Science Foundation of China (Grant No 52002317), Shaanxi Province Natural Science Foundation, China (Grant No. 2021JM-458), and Xi'an Science and technology Bureau (GXYD17.19).

References

1. C.J. Pei, J.J. Tan, Y. Li, G.G. Yao, Y.M. Jia, Z.Y. Ren, P. Liu, and H.W. Zhang, J. Adv. Ceram. 9[5] (2020) 588-594.
2. X. Zhang, Z. Jiang, B. Tang, Z.X. Fang, Z. Xiong, H. Li, C.L. Yuan, and S.R. Zhang, Ceram. Int. 46[8] (2020) 10332-10340.
3. S. Zhang, and R. Zuo, J. Alloys. Compd. 832 (2020) 154946.
4. S.Z. Hao, D. Zhou, F. Hussain, J.Z. Su, W.F. Liu, D.W. Wang, Q.P. Wang, and Z.M. Qi, J. Am. Ceram. Soc. 103[12] (2020) 7259-7266.
5. P. Zhang, M. Yang, M. Xiao, and Z.J. Zheng, Mater. Chem. Phys. 236 (2019) 121805.
6. G. Wang, H. Zhang, X. Huang, F. Xu, Y.M. Lai, G. Gan, Y. Yang, C. Liu, J. Li, and L.C. Jin, Mater. Lett. 235 (2019) 84-87.
7. C.J. Pei, G.G. Yao, Z.Y. Ren, J. Ceram. Process. Res. 17[7] (2016) 681-684.
8. T. Qin, C. Zhong, B. Tang, and S.R. Zhang, J. Eur Ceram. Soc. 41[2] (2021) 1342-1351.
9. Z.B. Feng, B.J. Tao, W.F. Wang, H.Y. Liu, H.T. Wu, and Z.L. Zhang, J. Alloys. Compd. 822 (2020) 153634.
10. G.G. Yao, Y. Li, J.J. Tan, C. Pei, Y. Zhang, and J. Chen, J. Ceram. Process. Res. 21[3] (2020) 338-342.
11. M. Castellanos, J. Gard, and A.R. West, J. Appl. Cryst. 15[1] (1982) 116-119.
12. L. Yuan, and J.J. Bian, Ferroelectrics. 387[1] (2009) 123-129.
13. J. Li, Z.W. Zhang, Y.F. Tian, L.Y. Ao, J.Q. Chen, A.H. Yang, C.X. Su, L.J. Liu, Y. Tang, and L. Fang, J. Mater. Sci. 55[33] (2020) 15643-15652.
14. X.C. Wang, X.P. Zhou, Y.X. Cao, Q. Wei, Z.Y. Zhao, and Y.H. Wang, J. Am. Ceram. Soc. 102[11] (2019) 6724-6731.
15. G.G. Yao, J.X. Yan, J.J. Tan, C.J. Pei, P. Liu, H.W. Zhang, and D.W. Wang, J. Eur. Ceram. Soc. 41[13] (2021) 6490-6494.
16. Y Zhan, L.X. Li, and M.K. Du, Ceram. Int. 47[19] (2021) 27462-27468.
17. M.A. Sanoj, C.P. Reshmi, and M.R. Varma, J. Am. Ceram. Soc., 92 [11] (2009) 2648-2653.
18. G. Wang, D. Zhang, Y. Lai, X. Huang, Y. Yang, G. Gan, F. Xu, Q. Wang, J. Li, C. Liu, L. Jin, Y. Liao, and H. Zhang, J. Alloys Compd. 782 (2019) 370-374.
19. P. Zhang, S.X. Wu, Y.G. Zhao, and M. Xiao, Mater. Chem. Phys. 222 (2019) 246-250.
20. Z.F. Fu, C. Li, J.L. Ma, and Y. Wu, Mater. Sci. Eng. B. 250 (2019) 114438.
21. X. Chu, J. Jiang, J.Z. Wang, Y.C. Wu, L. Gan and T.J. Zhang, Ceram. Int. 47[3] (2021) 4344-4351.
22. Z. Zhang, Y. Tang, H. Xiang, A. Yang, Y. Wang, C. Yin, Y. Tian, and L. Fang, J. Mater. Sci. 55[1] (2020) 107-115.
23. S.M. Zhai, P. Liu, S.S. Zhang, J. Eur. Ceram. Soc. 41[8] (2021) 4478-4483.
24. X. Zhang, B. Tang, Z. Fang, H. Yang, Z. Xiong, L. Xue, and S. Zhang, Inorg. Chem. Front. 5[12] (2018) 3113-3125.
25. C.J. Pei, C.D. Hou, Y. Li, G.G. Yao, Z.Y. Ren, P. Liu, and H.W. Zhang, J. Alloys. Compd. 792 (2019) 46-49.
26. G.G. Yao, J.J, Tan, J.X. Yan, M.Q. Liu, C.J. Pei, and Y.M. Jia, Ceram. Int. 47[19] (2021) 27406-27410.
27. M.K. Du, L.X. Li, S.H. Yu, Z. Sun, and J.L. Qiao, J. Am. Ceram. Soc. 101[9] (2018) 4066-4075.
28. E.S. Kim, B.S. Chun, R. Freer, and R.J. Cernik, J. Eur. Ceram. Soc. 30[7] (2010) 1731-1736.